JOURNAL OF GEOPHYSICAL RESEARCH, VOL. 99, NO. D10, PAGES 20,815–20,827, OCTOBER 20, 1994

The simulated Earth radiation budget of the National Center for Atmospheric Research community climate model CCM2 and comparisons with the Earth Radiation Budget Experiment (ERBE)

J. T. Kiehl, J. J. Hack, and B. P. Briegleb
National Center for Atmospheric Research, Boulder, Colorado

Abstract. This study documents the Earth radiation budget as simulated by the latest version of the National Center for Atmospheric Research community climate model (CCM2). The validation of the simulated Earth radiation budget is carried out through comparison with Earth Radiation Budget Experiment (ERBE) data. The study also documents the new cloud parameterization employed by CCM2. In general, the radiation budget of CCM2 is in better agreement with the ERBE data than previous versions of the CCM. In particular, the latitudinal structure of cloud radiative forcing is much improved over CCM1. The phase of the simulated seasonal cycle in top of atmosphere radiation quantities is well represented. In the tropics the magnitude is in good agreement with the observations from ERBE. In the northern hemisphere summer the model radiative properties contain a bias. In the shortwave spectral region the clouds reflect an insufficient amount of solar radiation, while in the longwave, too much radiation is emitted to space. These biases are associated with deficiencies in the cloud optical properties, namely, cloud liquid water path and cloud effective radius specification.

1. Introduction

Accurate simulation of the Earth radiation budget is one of the desired properties of a general circulation model, since the distribution of incoming and outgoing radiant energy is the primary forcing agent for the general circulation. Also, the change in the top of atmosphere radiative fluxes due to an external forcing defines the so-called climate sensitivity factor. This factor is important in identifying differences among general circulation models [*Cess et al.*, 1989]. One of the major determinants of the geographic distribution of the Earth radiation budget is the spatial and temporal distribution of cloud amount [e.g., *Ramanathan et al.*, 1989]. The forcing of the climate system by clouds is recognized as a key component to understanding the general climate system [*Ramanathan*, 1987]. For these reasons it is important to document a general circulation model's ability to accurately reproduce the magnitude and geographic distribution of incoming and outgoing radiant energy.

Over the past decade a series of general circulation models (GCMs), the community climate model (CCM), have been developed at the National Center for Atmospheric Research (NCAR). The radiation budget of the first version of the NCAR GCM (CCM0) was described by *Ramanathan et al.* [1983]. The radiation budget of the R15 version of the next version, CCM1, was described by *Smith and Vonder Haar* [1991], while the radiation budget of the T42 version of CCM1 was described by *Kiehl and Ramanathan* [1990]. The present study describes the Earth radiation budget simulation for the latest version of the community climate model (CCM2). Significant changes have been made in the model from CCM1 to CCM2 [see *Hack et al.*, this issue]. Indeed, virtually all model physics has changed from CCM1 to CCM2. Particularly relevant for the simulation of the Earth radiation budget are the changes in moist physics parameterizations and the radiation parameterizations.

In the past, limited global observational data made it difficult to quantify the accuracy of the simulated Earth radiation budget. With the availability of data from the Earth Radiation Budget Experiment (ERBE), model validation of the radiation budget has become far more quantitative. In this study we compare the simulated Earth radiation budget from CCM2 with data from the ERBE. Previous comparisons of the CCM to observations were confined to comparing monthly mean top of atmosphere fluxes for one or two months. In the present analysis the seasonal cycle of the Earth radiation budget will also be presented. The present simulation with CCM2 will be compared with the results from the study of *Kiehl and Ramanathan* [1990].

The paper is organized in the following manner. Section 2 describes the physical parameterizations in CCM2 particularly relevant to the simulated Earth radiation budget. Section 3 briefly describes the sources of observational data used for model validation. Section 4 presents results from the CCM2 and compares these with the observational data, where emphasis is on ensemble January and July results, and on the seasonal cycle of the Earth radiation budget; also included are regional analyses of the radiative fluxes by correlating longwave versus shortwave quantities. Finally, section 5 discusses the sources of identifiable biases between the model and observations and summarizes the findings.

Paper number 94JD00941.
0148-0227/94/94JD-00941$05.00

2. Model Description

A detailed description of the dynamical and physical structure of version 2 of the NCAR community climate

model (CCM2) is given by *Hack et al.* [1993]. A description of the climatology of CCM2 is given by *Hack et al.* [this issue]. We briefly describe the cloud and radiation parameterizations employed in CCM2. Further details can be found in the work by *Hack et al.* [1993]. The NCAR community climate model (CCM) is a spectral general circulation model. The standard resolution of the model is T42 (equivalent to 2.8° by 2.8° in latitude and longitude) with 18 layers in the vertical. A major radiative difference between CCM2 and CCM1 is that CCM2 has a diurnal cycle. Solar and longwave fluxes are calculated every hour. The model time step at the standard model resolution of T42 is 20 min. The solar and longwave fluxes are held fixed for time steps between the hourly radiation calculations. For the longwave calculations the absorptivity and emissivity for the clear sky fluxes are calculated every 12 hours. The effects of clouds on the radiative fluxes are calculated every hour.

The clear sky longwave radiation model in CCM2 is nearly identical to that used in CCM1 [see *Kiehl et al.*, 1987], except for the inclusion of the Voigt line shape effect for CO_2 and O_3 [*Kiehl and Briegleb*, 1991]. With regard to the longwave properties of clouds, the one difference with CCM1 is that the cloud emissivity is given as

$$\varepsilon = 1.0 - e^{-0.1\mathrm{LWP}} \tag{1}$$

for all cloud types. LWP (grams per square meter) is the cloud liquid water path for a given model layer. In CCM1 a version of (1) was applied only to stratiform clouds associated with deep convection. The 0.1 factor in (1) includes a diffusivity factor of 1.66, so the longwave cloud absorption coefficient is 0.06 $m^2\ g^{-1}$. This value falls within the range of current observational estimates, where for liquid clouds see *Chylek and Ramaswamy* [1982] and for ice clouds see *Ebert and Curry* [1992]. Clouds are assumed to be randomly overlapped for longwave computations.

The CCM1 solar radiation model has been replaced in CCM2 with a δ-Eddington scheme described by *Briegleb* [1992]. The solar spectrum is divided into 18 spectral intervals. Gas absorption is treated by the exponential sum method. Briegleb shows comparisons of this model with the more detailed line-by-line adding-doubling results of *Ramaswamy and Friedenreich* [1991]. Errors in heating rates are in general less than a few tenths of a degree per day. The cloud optical properties are accounted for by using the *Slingo* [1989] parameterization, which relates the extinction optical depth, the single-scattering albedo, and the asymmetry parameter to the cloud liquid water path and the cloud drop effective radius (see below). Cloud overlap is accounted for by scaling the cloud extinction optical depth by $A_c^{3/2}$, where A_c is the cloud fraction in a given model layer. This scaling acceptably reproduces heating rates and fluxes from the random overlap assumption [see *Briegleb*, 1992].

The cloud fraction scheme is a generalization of that proposed by *Slingo* [1987], which was developed using data from the Global Atlantic Tropical Experiment (GATE). The approach is diagnostic in that cloud fraction is determined by large-scale variables (i.e., relative humidity, atmospheric stability, vertical velocity, and the convective precipitation rate). Three types of clouds are diagnosed: convective cloud, stratiform cloud, and low-level marine stratus. The differences with the original Slingo scheme are clouds are allowed to form in any tropospheric model layer (except for the model layer nearest the surface), nonprecipitating convective clouds have a total cloud fraction of 20%, low-level stratiform clouds occur in the presence of any upward vertical velocity, and the relative humidity thresholds for stratiform cloud formation are stability dependent. The assumption that clouds do not form in the lowest model layer is historical in origin. The earlier versions of the CCM had excessive moisture in the lowest model layer, associated with deficient boundary layer processes. Attempts to allow for clouds in the lowest model layer resulted in excessive low cloud cover. Recent studies with CCM2 indicate that this does not occur in this version of the model. Hence future versions of the CCM will allow for clouds in the lowest layer.

The total convective cloud amount occurring between N contiguous model levels undergoing convection is given by

$$\bar{A}_{\mathrm{con}} = 0.20 + 0.125 \ln (1.0 + P) \tag{2}$$

where P is the convective precipitation rate in millimeters per day. The total convective cloud amount is not allowed to exceed 0.80. Equation (2) accounts only for convective cloud; cirrus outflow associated with deep convection is modeled by the large-scale stable formulation (8). The convective cloud amount within each of the N contiguous layers is assumed to be randomly overlapped within the layers. Thus the fractional amount of convective cloud within each layer is

$$A_{\mathrm{con}} = 1.0 - (1.0 - \bar{A}_{\mathrm{con}})^{1/N} \tag{3}$$

The assumption of random overlap is perhaps least applicable to convective clouds. A maximum overlap assumption would be more appropriate. Current GCMs have yet to account for various types of overlap for differing cloud configurations. The large-scale relative humidity is adjusted to account for the assumption that the area covered by convective clouds is saturated,

$$\mathrm{RH}' = \frac{\mathrm{RH} - A_{\mathrm{con}}}{1.0 - A_{\mathrm{con}}} \tag{4}$$

In levels below levels p = 750 mbars low-level stratiform cloud cover is defined as

$$A_c = \left(\frac{\mathrm{RH}' - 0.9}{0.1}\right)^2 \qquad \omega < 0 \tag{5}$$

where ω is the vertical velocity in millibars per second.

Stratus associated with low-level inversions (e.g. marine stratus) is defined by

$$A_c = 0 \qquad \mathrm{RH}' < 0.6 \tag{6a}$$

$$A_c = \left(-6.67 \frac{\partial \theta}{\partial p} - 0.667\right)\left(1.0 - \frac{0.9 - \mathrm{RH}'}{0.3}\right) \cdot \left(\frac{p - 750}{150}\right) \tag{6b}$$

$$0.6 \le \mathrm{RH}' \le 0.9,\ \partial\theta/\partial p < -0.125°\mathrm{K\ mbar}^{-1},$$

$$750\ \mathrm{mbar} \le p \le 900\ \mathrm{mbar}$$

$$A_c = \left(-6.67 \frac{\partial \theta}{\partial p} - 0.667\right)\left(\frac{p - 750}{150}\right) \tag{6c}$$

$$\mathrm{RH}' > 0.9,\ \partial\theta/\partial p < -0.125°\mathrm{K\ mbar}^{-1},$$

$$750\ \mathrm{mbar} \le p \le 900\ \mathrm{mbar}$$

where $\partial\theta/\partial p$ is the maximum inversion strength. The pressure factor, $((p - 750)/150)$, accounts for the transition from boundary layer cloud associated with low-level inversions to other types of low-level stratiform clouds described by (5). Mid- and high-level stratiform cloud amount is defined to occur between 750 mbar and an upper level pressure defined by,

$$P_{\text{top}} = 250 - 165 \cos^2 \phi, \tag{7}$$

where ϕ is latitude.

The stratiform cloud for $750 \geq p \geq P_{\text{top}}$ is defined by

$$A_c = \max\left\{0, \left[\frac{\text{RH}' - \text{RH}_{\text{lim}}(p, \phi)}{1 - \text{RH}_{\text{lim}}(p, \phi)}\right]^2\right\} \tag{8}$$

where

$$\text{RH}_{\text{lim}}(p, \phi) = 0.999 - 0.10\left[1.0 - \frac{N^2}{2.5 \times 10^{-4}}\right] \tag{9}$$

and N^2 is the square of the Brunt-Vaisalla frequency,

$$N^2 = -\frac{g^2 p}{\theta}\frac{\partial\theta}{\partial p}. \tag{10}$$

The ratio of $N^2/2.5 \times 10^{-4}$ is not allowed to exceed 1. The P_{top} factor was used to bound the clouds before the stability dependent critical relative humidity factor was implemented in CCM2. Recent studies where clouds are allowed to form independent of P_{top} indicate no significant change in the model climatology. Future versions of the CCM will not employ this limit to cloud cover.

Finally, the cloud in each layer is defined as

$$A_c^T = (1.0 - A_{\text{con}})A_c + A_{\text{con}} \tag{11}$$

where A_c^T is not allowed to exceed 0.999. Figure 1a shows the zonally averaged cloud cover for January based on this parameterization. Figure 1b shows the zonally averaged effective cloud cover, i.e., εA_c^T, for January.

The in-cloud liquid water content is obtained from a specified profile,

$$\rho_\ell = \rho_\ell^0 \exp(-z/h_\ell) \quad \text{g m}^{-3} \tag{12}$$

where z is altitude above the surface in meters, the large-scale liquid water reference value ρ_ℓ^0 is equal to 0.18 g m^{-3}, and h_ℓ is a liquid water scale height defined as

$$h_\ell = 1080 + 2000 \cos^2 \phi \text{ m}. \tag{13}$$

The in-cloud liquid water path for a cloud between layers z_k and z_{k+1} is given by

$$\text{LWP}(k) = \int_{z_k}^{z_{k+1}} \rho_\ell(z)\, dz$$

$$= \rho_\ell^0 h_\ell [e^{-z_{k+1}/h_\ell} - e^{-z_k/h_\ell}] \quad \text{g m}^{-2} \tag{14}$$

Note that although LWP is defined as the liquid water path, it also accounts for the ice water path. A zonal cross section of the in-cloud liquid water path for the July simulation of CCM2 is shown in Figure 2. The peak in-cloud liquid water path for each model level is located in the tropics near 800 mbar with a magnitude of 80 g m^{-2}. Note that the model levels are indicated by the internal tick marks in Figure 2. The latitude dependence in h_ℓ ensures that the liquid water concentration (and hence path) decreases monotonically towards the poles. In-cloud liquid water paths in the tropics above 200 mbar are less than 10 g m^{-2}. Note that the grid box–averaged cloud liquid water path is obtained by multiplying the value from (14) by the cloud fraction. The cloud radiative parameters also depend on the cloud drop effective radius, r_{eff}. In CCM2, r_{eff} = 10 μm for all clouds. The implications of assumptions (12) and a universal 10 μm effective drop size are discussed further in section 5.

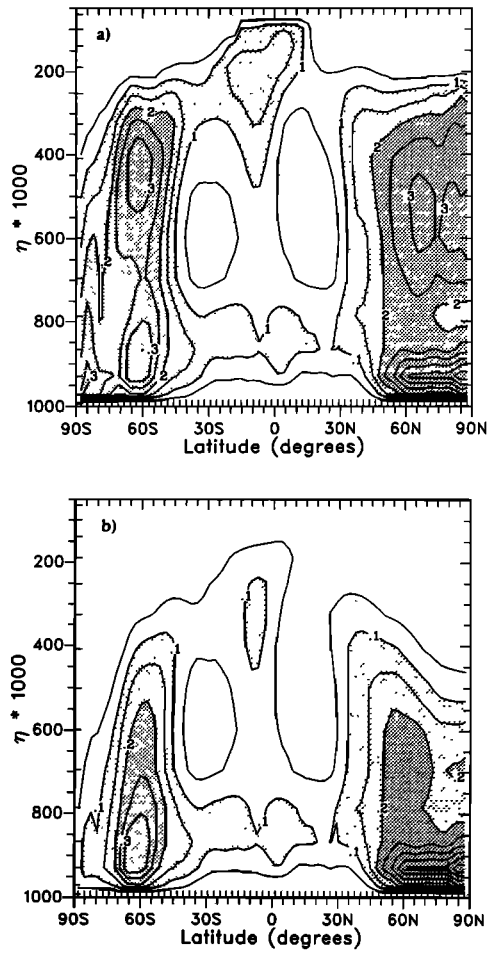

Figure 1. CCM2 January ensemble zonally averaged (a) cloud fraction and (b) effective cloud fraction (i.e., emissivity times cloud fraction). Here 1000η is approximately equal to the pressure in millibars.

3. Model and Observational Data Used in Comparison

The model data are obtained from a 20-year seasonal control integration of CCM2 at T42 resolution (approximately 2.8° × 2.8° grid resolution). The annually repeating sea surface temperatures for this simulation are from the climatology of *Shea et al.* [1990]. Other boundary data sets are described by *Hack et al.* [1993]. The model top is at 2.9 mbar. All model results reported here are based on 20 monthly mean samples which make up the ensemble means.

For Earth radiation budget comparisons we use multiyear

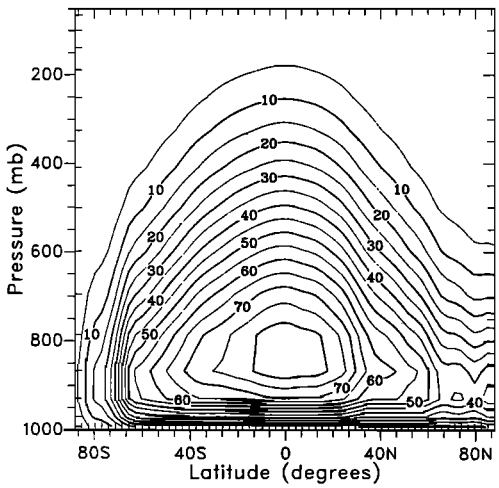

Figure 2. CCM2 July zonally averaged cloud liquid water path (equation (14)) in grams per square meter per layer.

means of radiation quantities from the NASA Earth Radiation Budget Experiment (ERBE). The years included in the averages are for July 1985, 1986, and 1988. For January we use monthly mean ensemble averages of the two years 1986 and 1988. We removed 1987 from the ensemble monthly means since it was an anomalous year due to the strong El Nino. Since the standard CCM2 employs climatological mean sea surface temperatures, the strong El Nino signal is not present in the forcing data. For the seasonal cycle results we have also eliminated 1987 from the ERBE analysis.

The ERBE provides monthly mean data on a 2.5° × 2.5° grid. The data used in the present comparison are the outgoing longwave radiation (OLR), the planetary albedo, the clear sky outgoing longwave flux, and the clear sky albedo. A detailed description of how these data are determined and archived is given by *Barkstrom* [1984], *Barkstrom and Smith* [1986], *ERBE Science Team* [1986], and *Ramanathan et al.* [1989]. Further comments on the retrieval of the clear sky fluxes are given by *Kiehl and Ramanathan* [1990]. The data used in the present comparison have been formatted in the same manner as the CCM2 data [*Hurrell and Campbell*, 1992]. The estimated uncertainty in the fluxes is ±10 W m^{-2}, while cloud forcing data poleward of 60° south and north are quite uncertain.

One advantage in using the ERBE data is the existence of the retrieved clear sky flux. This flux, in conjunction with the total radiative flux, defines the cloud radiative forcing. In the longwave, cloud radiative forcing is defined as

$$\text{LWCF} = F_{\text{clr}} - F_{\text{tot}} \tag{15}$$

where F_{clr} is the clear sky outgoing longwave radiative (OLR_{clr}) flux and F_{tot} is the actual OLR. Since for most cases the clear sky outgoing flux is larger than the total flux, LWCF is positive, indicating that clouds warm the surface-atmosphere system in the longwave. In the shortwave spectral region, the cloud forcing is defined as

$$\text{SWCF} = S_{\text{tot}} - S_{\text{clr}} \tag{16}$$

where S_{tot} is the net solar absorbed flux in the surface-atmosphere system, and S_{clr} is the clear sky solar absorbed flux of the system. Since the net includes the effects of clouds, this quantity is in general smaller than the clear sky absorbed flux. Hence the shortwave cloud forcing is, generally, negative, indicating that clouds tend to cool the surface-atmosphere system.

A problem in using the cloud radiative forcing is that for certain geographic regions, there are no identifiable clear sky days for an entire month. Thus the clear sky fluxes contain regions of missing data. Note that the number of missing data are different for the longwave and shortwave fluxes due to differences in retrieval algorithms. When multiple years are combined to create an ensemble month, the missing data regions for the ensemble are even more numerous. Although initially this may raise some concern, in practice the missing data regions are sufficiently small that the cloud radiative forcing is still a useful diagnostic. Indeed, we show in the present study that zonal means in LWCF and SWCF differ by less than 5 W m^{-2} when missing data regions are included.

4. Comparison of Model Results to Satellite Data

The comparisons of the radiative energy budget between the CCM2 and the ERBE data will include global means, geographic distributions, zonal means, and regional statistics. All model results are based on the 20-year ensemble control integration of CCM2. All ERBE results are based on the 2- or 3-year ensemble averages as defined in the previous section.

Global Comparisons

Globally averaged top of atmosphere fluxes and related cloud properties are presented in Tables 1 and 2. Table 1 presents the 20-year annual mean averages of the radiative flux quantities. These include the outgoing longwave radiation (OLR), the absorbed shortwave flux, planetary albedo, the clear sky flux equivalents, and the longwave and shortwave cloud forcing as defined in (15) and (16).

The globally annual averaged total cloud cover, assuming random overlap, is 0.53 from CCM2. Note that the model surface-atmosphere system absorbs 8 W m^{-2} more solar flux than it emits to space in the longwave. This imbalance was not "tuned" out of the model, since there are known biases in the shortwave cloud forcing. As will be shown in the discussion on geographic and regional results, the clouds in CCM2 reflect an insufficient amount of solar radiation back to space. Recent work by *Kiehl* [1994a] indicates that this is due to deficiencies in the specified cloud optical properties. When these deficiencies in optical properties are addressed, this bias in the current version of CCM2 is mainly eliminated. In the longwave, CCM2 does not include the radiative

Table 1. Global Annual Averaged Earth Radiation Budget Quantities From the CCM2 and ERBE

Field	CCM2	ERBE
OLR, W m^{-2}	240.5	234.8
S_{tot}, W m^{-2}	248.4	238.1
Albedo	0.28	0.30
OLR_{clr}, W m^{-2}	271.4	264.0
S_{clr}, W m^{-2}	295.2	286.3
LWCF, W m^{-2}	30.9	29.2
SWCF, W m^{-2}	−46.8	−48.2

effects of trace gases such as methane, nitrous oxide, and the chlorofluorocarbons (CFCs). Inclusion of these gases, at present gas concentrations, would reduce the globally averaged OLR value by approximately 2 W m^{-2}.

Table 2 presents results for January and July ensemble averages from CCM2 and from the ERBE data. In January the net imbalance between incoming and outgoing radiative flux is 17.4 W m^{-2}, while in the ERBE data this imbalance is 10 W m^{-2}. In July the net imbalance in CCM2 is −3.0 W m^{-2}, while in the ERBE data it is −10.5 W m^{-2}. The globally averaged longwave and shortwave cloud forcing in CCM2 for January agrees to within less than 3 W m^{-2} with the ERBE data. In July there is a 7 W m^{-2} difference in the SWCF between the model and the ERBE result. The indication is that the model clouds reflect less radiation back to space than suggested by the observations.

Geographic and Zonal Comparisons

The geographic distributions of outgoing longwave radiation for January and July from CCM2 and ERBE are shown in Figures 3a–3d. In January the ERBE OLR in the tropical western Pacific is less than 220 W m^{-2} over a very broad region from 60°E to the dateline, and from roughly 5°N to 15°S. In CCM2 the region of OLR less than 220 W m^{-2} is much smaller, essentially confined over Indonesia. The low-OLR regions over the Congo and Brazil associated with deep convective activity are better represented in the model. The maxima in OLR associated with the dry and warm subsidence regions are roughly 10 W m^{-2} larger in the model than in the ERBE data. This is in part due to the lack of trace gas absorption [see *Kiehl and Briegleb*, 1992] and also in part due to less column water vapor [see *Hack et al.*, this issue]. Compared to the results from CCM1 [*Kiehl and Ramanathan*, 1990], there has been a substantial improvement in the simulated OLR. This is due to a moister atmosphere (linked to improvements in the planetary boundary layer and convection parameterization; see *Hack* [1994] for more details) and improvements in the cloud parameterization. In July, similar biases exist in the tropical western Pacific region. In particular, over the Indian subcontinent the ERBE data show this entire region with low OLR (less than 220 W m^{-2}) associated with the monsoon, while the model simulation does not show this feature. Also note that over the northern hemisphere landmasses the simulated OLR is larger (by 40–50 W m^{-2}) than the ERBE data. This is directly related to the warm summer northern hemisphere surface temperature bias described by *Hack et al.* [this issue]. In July the CCM2 land surface temperatures are

Table 2. Seasonal Globally Averaged Earth Radiation Budget Quantities From the CCM2 and ERBE

	January		July	
Field	CCM2	ERBE	CCM2	ERBE
OLR, W m^{-2}	236.4	232.6	248.0	238.7
S_{tot}, W m^{-2}	253.8	242.6	245.0	228.2
Albedo	0.28	0.31	0.26	0.31
OLR_{clr}, W m^{-2}	267.4	260.6	276.6	266.9
S_{clr}, W m^{-2}	305.1	294.9	287.0	277.2
LWCF, W m^{-2}	31.0	28.0	28.6	28.2
SWCF, W m^{-2}	−51.3	−52.3	−42.0	−49.0

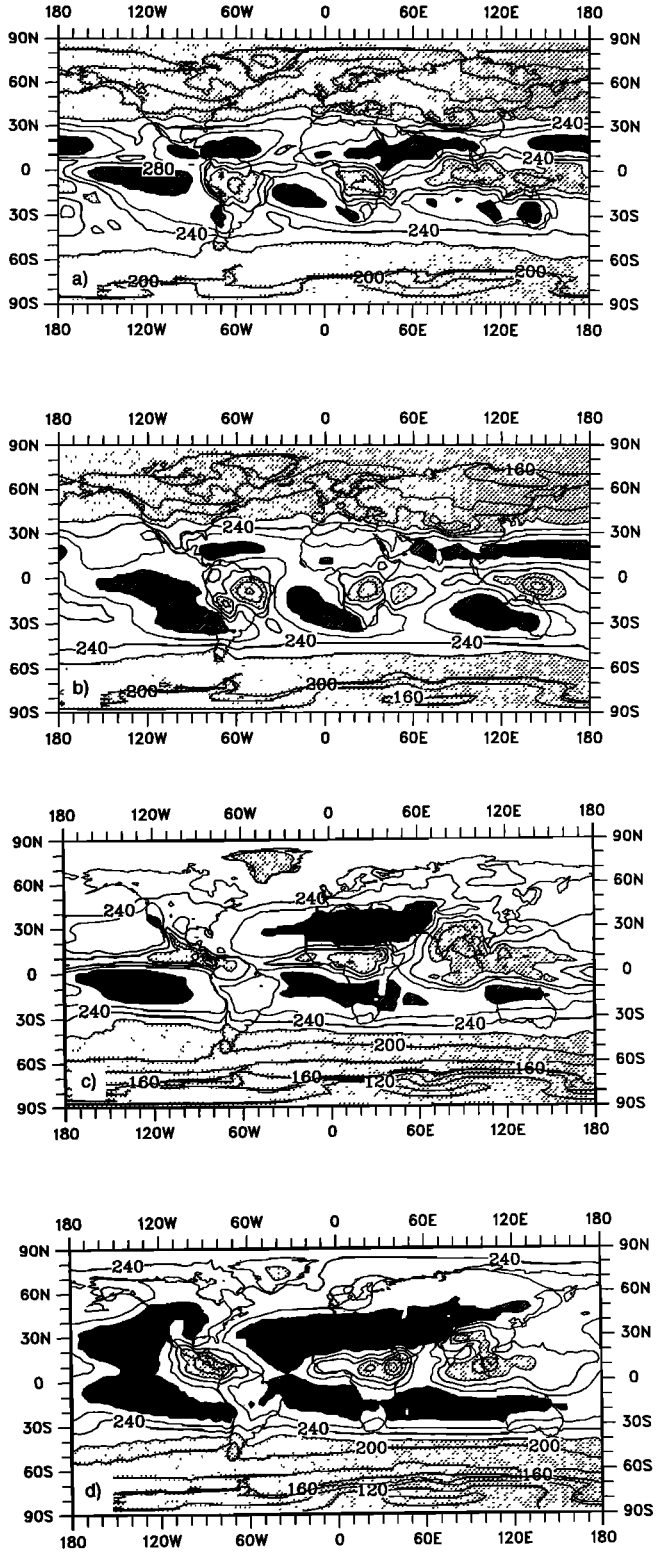

Figure 3. Geographic distribution of outgoing longwave radiation (watts per square meter) for (a) January ERBE (b) January CCM2, and (c) July ERBE and (d) July CCM2. Contour interval is 20 W m^{-2}. Hatched regions denote OLR greater than 280 W m^{-2}, stippled regions OLR less than 220 W m^{-2}.

6°–10°K higher than the climatological values. As discussed in section 5, this bias is a result of deficiencies in the cloud optical properties.

The zonally averaged OLR for January and July from CCM2 and ERBE is shown in Figures 4a–4b. In January, in the northern hemisphere the model is in very good agreement with the ERBE observations. In the tropics the model overestimates the observations by roughly 10 W m^{-2}. Some of this bias can be ascribed to the lack of trace gases such as CH_4, N_2O, and the CFCs, but much of the bias is related to upper level clouds that are too transparent, i.e., their emissivity is too low. In July the simulated OLR in the southern hemisphere is in good agreement with the ERBE data. In the tropics, as in January, the model overestimates the OLR, while in the summer hemisphere, the simulated OLR is roughly 20 W m^{-2} larger than the ERBE observations. As discussed above, this latter bias is due to the warm simulated land surface temperatures.

Figures 5a–5d show the January and July geographic distribution in planetary albedo from the model and the ERBE data. The January albedo of the model agrees well with the ERBE results in the three deep convective regions in the tropics. However, in the Indian Ocean the albedo simulated by the model is less than 0.3, while the observed albedo is between 0.3 and 0.4. This underestimation is albedo is related to an underprediction in cloud amount. The high albedo in the model's eastern Pacific Intertropical

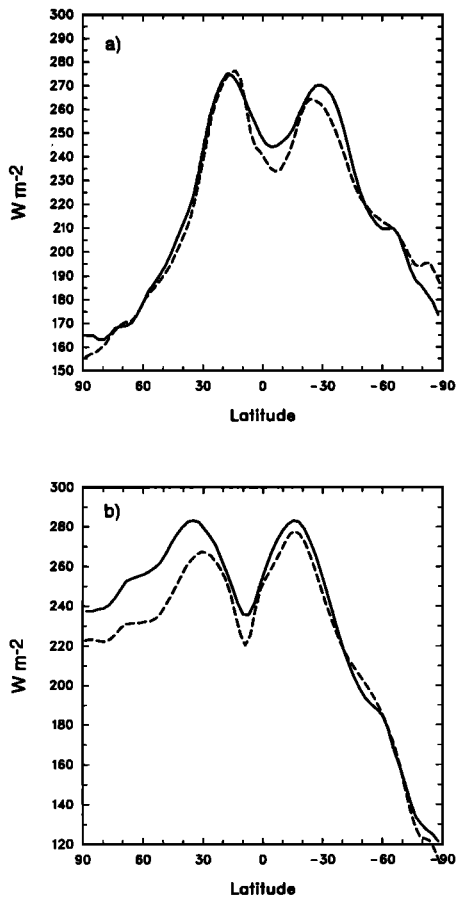

Figure 4. Zonally averaged OLR (W m^{-2}) from ERBE (dashed curves) and CCM2 (solid curves) for (a) January and (b) July.

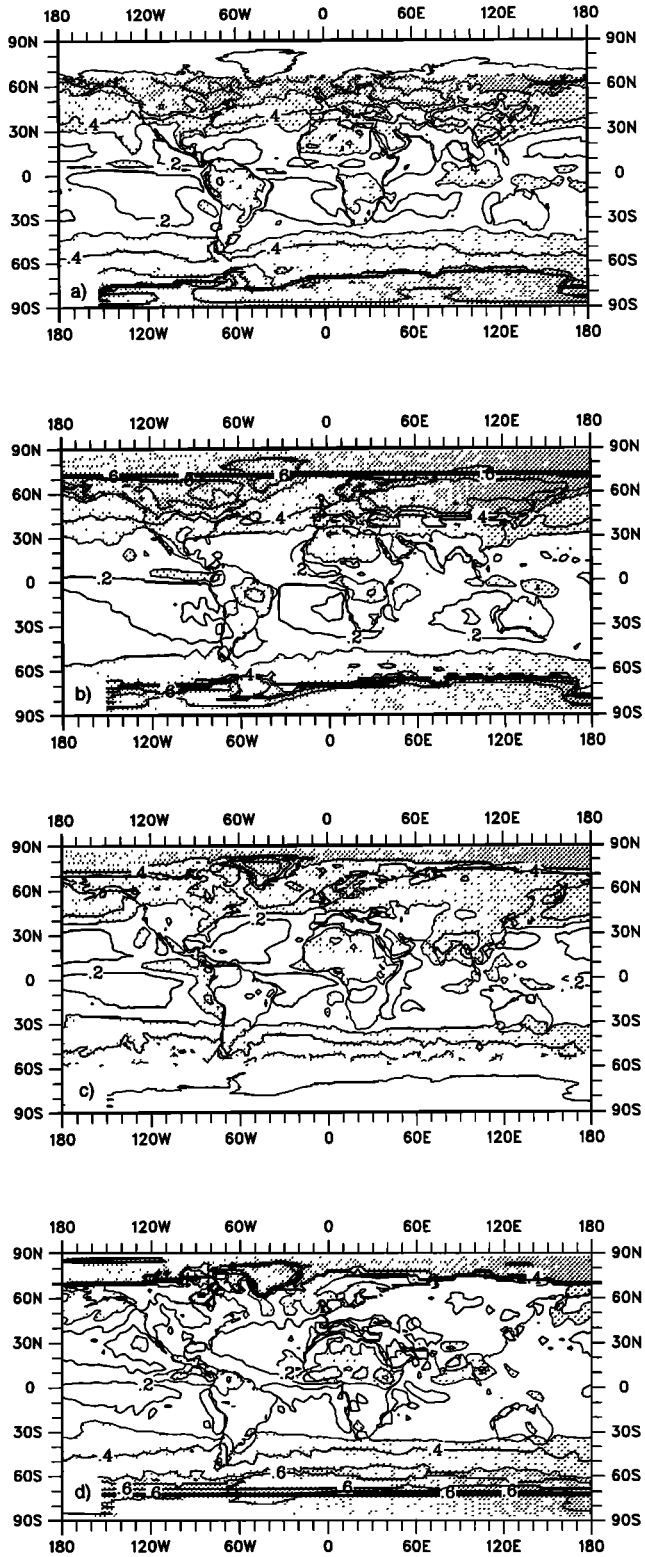

Figure 5. Geographic distribution of planetary albedo for (a) January ERBE, (b) January CCM2, (c) July ERBE, and (d) July CCM2. Contour interval is 0.1. Light stippling indicates regions greater than 0.3; heavy stippling indicates regions with albedos greater than 0.5.

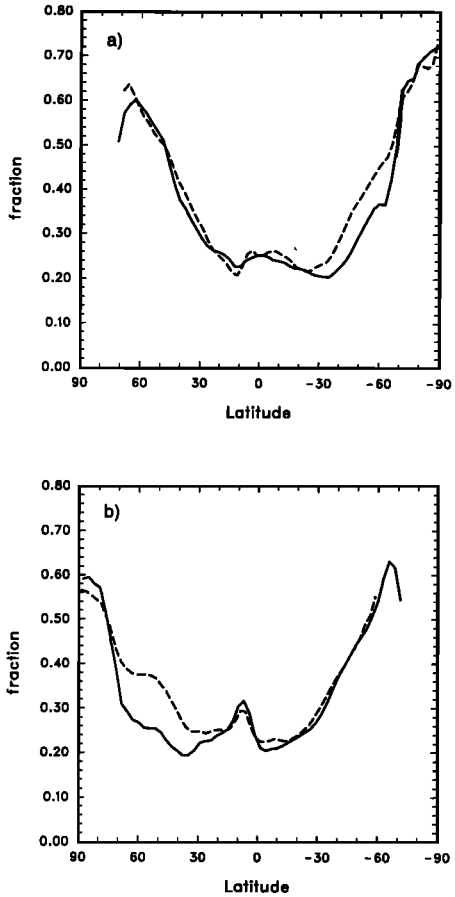

Figure 6. Zonally averaged planetary albedo from ERBE (dashed curves) and CCM2 (solid curves) for (a) January and (b) July.

Convergence Zone (ITCZ) is much more distinct than in the ERBE data. This "bright band" is due mostly to low (pressures greater than 800 mbar in height) cloud cover. The ERBE albedo patterns off the coasts of the western United States, South America, and southern Africa clearly indicate the presence of marine stratus cloud. In the model there is a clear signature of these clouds off the coasts of the United States and southern Africa, but far smaller albedos off the coast of South America. Finally, the albedo in the southern hemisphere at 60°S is lower in the model than in the ERBE data (by 20%).

In July the simulated albedo over northern hemisphere landmasses is too low compared to the ERBE data (0.2 compared to 0.3). The model simulates the marine stratus clouds off the coast of California, but fails to adequately capture the stratus off of South America and southern Africa. Elsewhere there is good agreement between the simulated albedo and the observed.

Figures 6a and 6b show the zonally averaged planetary albedo for January and July. There is very good agreement between the model and the observations for the winter hemispheres. In the summer hemispheres the model albedo is up to 30% too low. As previously discussed, this is due to deficiencies in the prescribed cloud optical properties.

The radiative effects of clouds become more apparent when we consider the cloud radiative forcing. Figures 7a–7d show the longwave cloud forcing from CCM2 and the ERBE

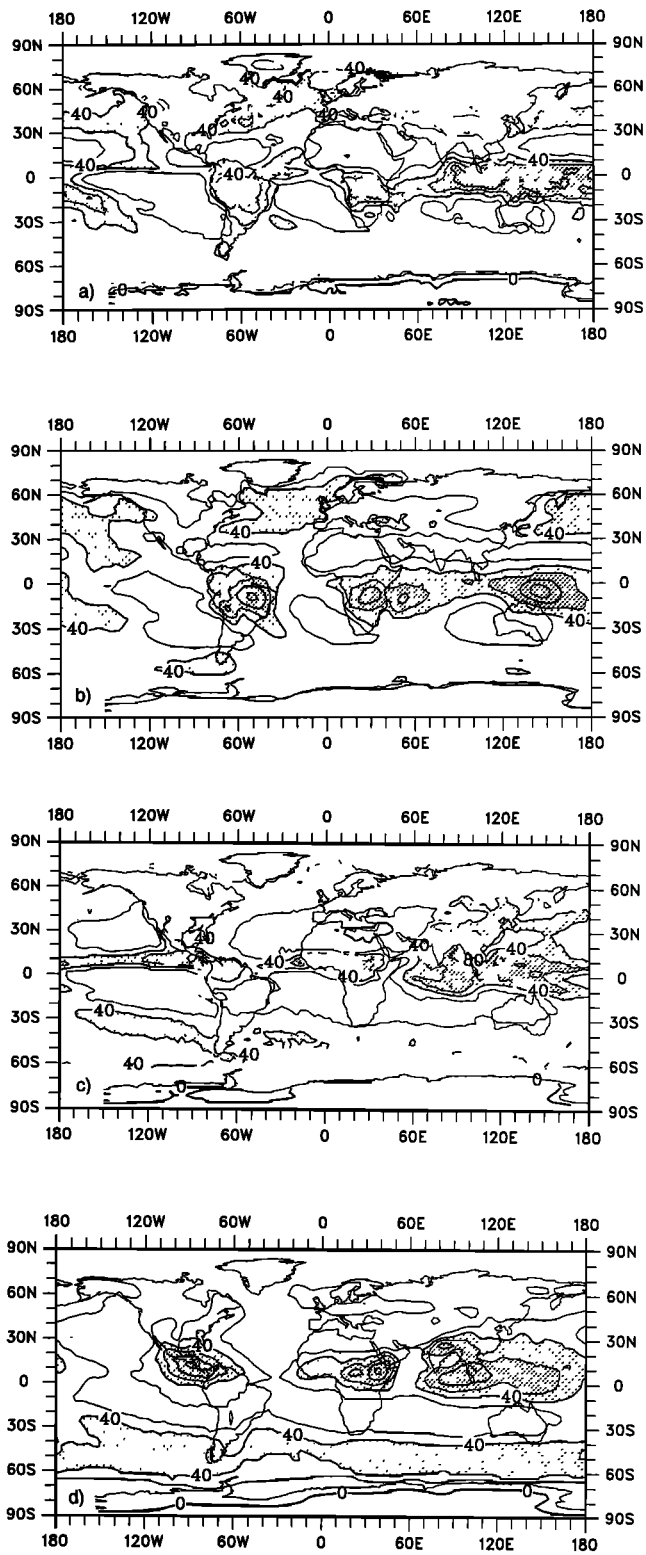

Figure 7. Geographic distribution of longwave cloud forcing (watts per square meter) for (a) January ERBE, (b) January CCM2, (c) July ERBE, and (d) July CCM2. Contour interval is 20 W m^{-2}. Light stippling indicates LWCF greater than 40 W m^{-2}, heavy stippling, LWCF greater than 60 W m^{-2}.

data for January and July conditions. Note, as discussed in section 3, that in the case of the ERBE data there are areas of missing data. Unfortunately, these are just the regions where knowledge of the cloud radiative forcing is of great interest. The contour plots of these fields actually make it appear that more data are missing, since contouring requires neighboring points for plotting. Since monthly averages include more than one year's data, missing data are quite prevalent in regions of high cloudiness (e.g., the regions of deep convective activity in the tropics). Despite these regions of missing data, a number of interesting features are apparent in both model and observations. In the tropics the model is capturing the correct location and seasonal shifts of the three regions of deep convective activity. The ITCZ feature in the ERBE data is quite distinct across both the Pacific and the Atlantic, while absent in the model. This is due to a lack of high cloud in these regions. Although there is a distinct band of low cloud associated with the ITCZ, there is no distinct band in mid- or high-level cloud associated with the ITCZ. Simulations of CCM2 at higher horizontal resolutions (T63 and T106) indicate that the radiative features associated with the ITCZ improve with higher resolution.

Figures 8a and 8b show the zonal average of the longwave cloud forcing from CCM2 and ERBE for January and July, respectively. Note that since the ERBE data have a number of missing data regions, we have masked the CCM2 results with these ERBE-defined missing data. We also show the unmasked data for comparison. There is little difference between the masked and unmasked results. However, this is due mainly to a mismatch between the ERBE-masked regions and the exact location of large LWCF from the model. The latitudinal structure of the LWCF in January agrees very well with the ERBE results. This is a significant improvement over the results of CCM1 shown in the work by *Kiehl and Ramanathan* [1990], where there was little latitudinal structure present. Indeed, there is now more latitudinal structure in CCM2 than in the ERBE data. In July there is a distinct underestimation in the model's LWCF in the northern hemisphere compared to ERBE. In the southern hemisphere the model overestimates the LWCF. As discussed in section 5, the northern hemisphere bias is related to the cloud optical property prescription.

Figures 9a–9d show the geographic distribution of shortwave cloud forcing from CCM2 and the ERBE data for January and July. For the shortwave cloud forcing, there is a well-defined band of large SWCF in the ITCZ region in both observations and model. As noted above, the model predicts a well-defined band of low cloud cover in the ITCZ, and it is this cloud type that is contributing most to the SWCF. Note that if the model predicted more upper level cloud cover, this would also create this type of feature. Hence we cannot discern from the ERBE data alone which cloud type is contributing most to this feature. *Kiehl* [1994b] has argued based on a comparison of ERBE and ISCCP data that this feature is more likely due to high cloud cover. In July the model predicts marine stratus off the coast of California and the Baja peninsula, which is also present in the ERBE July data. In January the model predicts marine stratus cloud type off of the coast of Angola, which is also present in the observations. However, in this region the cloud forcing is slightly larger in the observations than predicted by the model. The model does not adequately represent the marine stratus off the coast of Chile in either season. This is believed to be related to numerical representation problems associated with the orography of the Andes. Indeed, a spectral "ringing" effect is apparent in the January SWCF in this region. In July, over northern hemisphere continental regions there is a severe underestimation of SWCF in the model (as large as 50–60 W m^{-2}). This bias has been addressed by *Kiehl* [1994a].

The zonally averaged January and July shortwave cloud forcing for CCM2 and ERBE is shown in Figures 10a and 10b. Again, the model zonal means employ the missing data regions of ERBE. The northern hemisphere July bias is quite apparent in these results. Note that this bias appears generally in the summer hemisphere.

To fully see the amplitude of the seasonal cycle in the Earth radiation budget, we have calculated the difference of the monthly mean radiation field (e.g., OLR, albedo, etc.) from its annual mean value. The zonal means of these fields are then presented as a function of latitude versus month. Figures 11a and 11b show the seasonal cycle of the amplitude of the outgoing longwave radiation. There is good agreement in the morphology of the OLR during the transition seasons. In the subtropics and tropics the model's OLR amplitude is up to 10 W m^{-2} smaller than the ERBE amplitude, while in the northern hemisphere

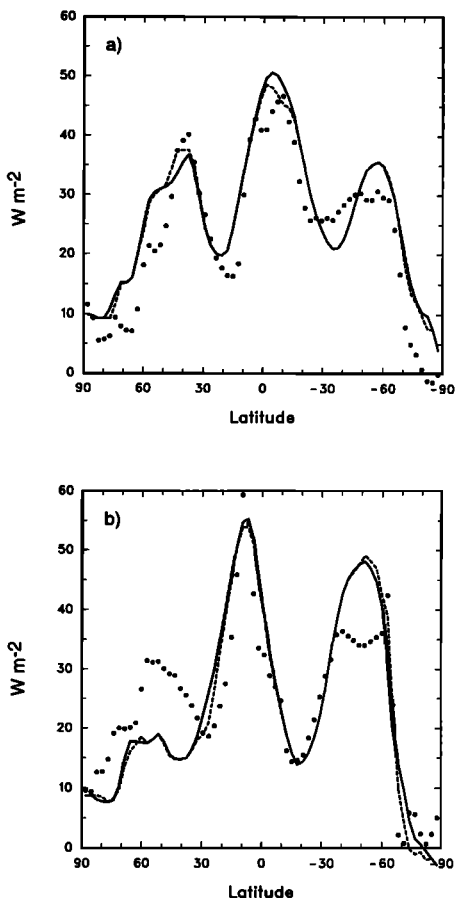

Figure 8. Zonally averaged longwave cloud forcing (watts per square meter) from ERBE (solid circles), CCM2 unmasked (solid curves), and CCM2 masked by ERBE missing data (dashed curves) for (a) January and (b) July.

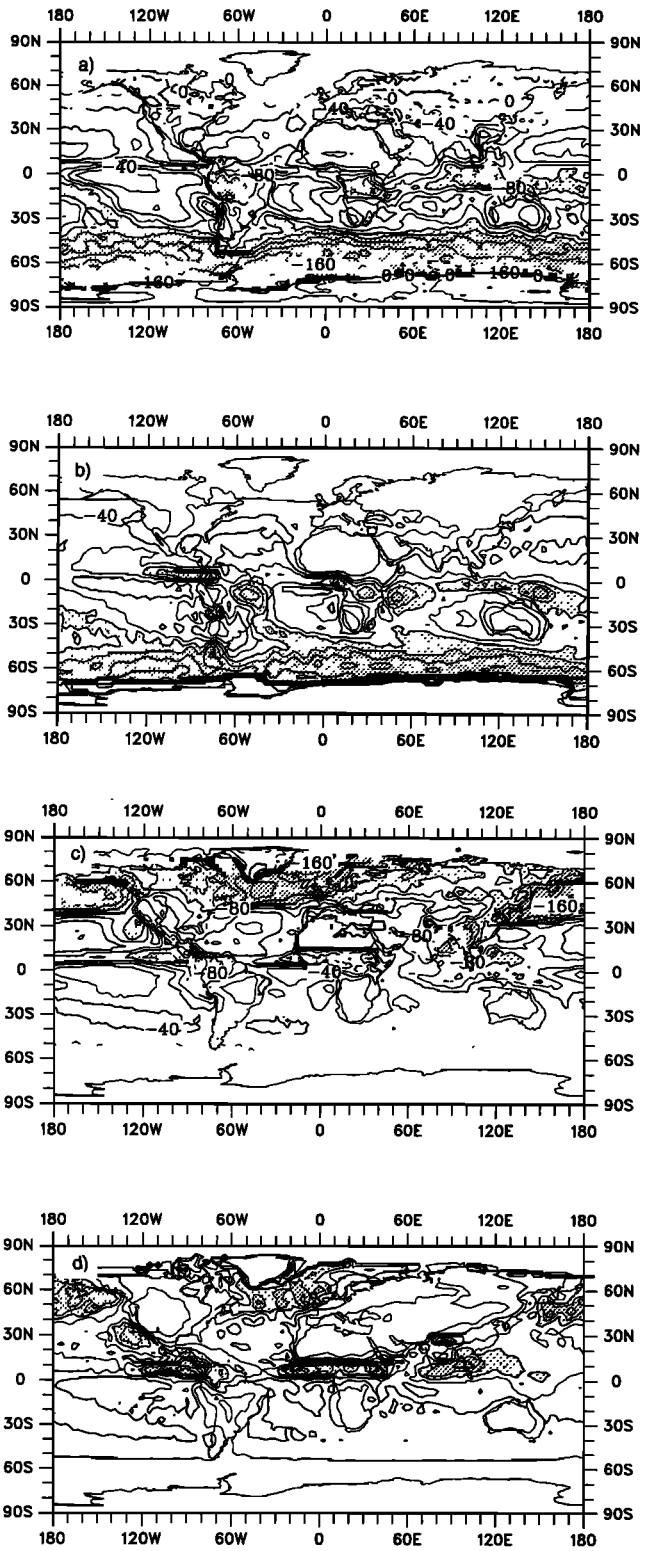

Figure 9. Geographic distribution of shortwave cloud forcing (watts per square meter) for (a) January ERBE, (b) January CCM2, (c) July ERBE, and (d) July CCM2. Contour interval is 20 W m^{-2}. Light stippling indicates SWCF greater than 40 W m^{-2}; heavy stippling SWCF greater than 60 W m^{-2}.

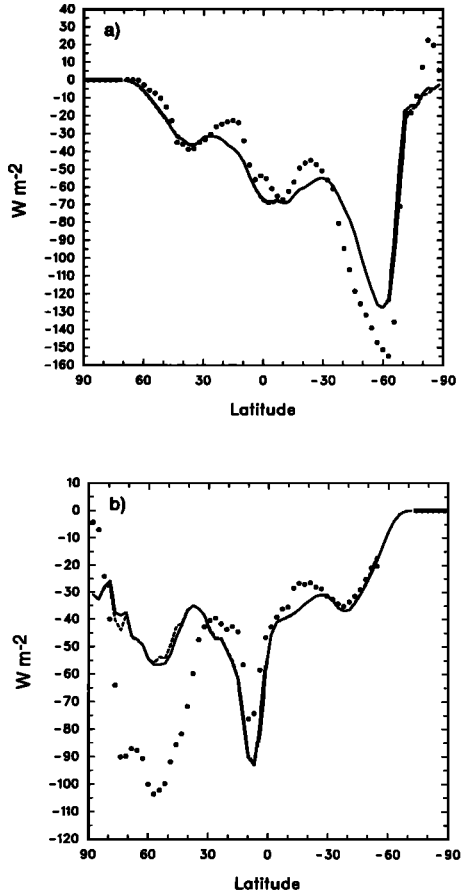

Figure 10. Zonally averaged shortwave cloud forcing (watts per square meter) from ERBE (solid circles), CCM2 unmasked (solid curves), and CCM2 masked by ERBE missing data (dashed curves) for (a) January and (b) July.

extratropics the model amplitude is 14 W m^{-2} too large compared to ERBE. The model's southern hemisphere amplitude agrees to within a few watts per square meter with the ERBE results. The seasonal amplitude in planetary albedo is shown in Figures 12a and 12b. Again the morphology of the seasonal cycle is well represented in the model. However, the amplitude is larger in the model than in the observations. The seasonal cycle in solar absorbed flux is dominated by the seasonal cycle in solar insolation; hence the comparison conveys little information. Figures 13a and 13b show the seasonal cycle in the amplitude of the LWCF from both CCM2 and ERBE, respectively. The difference between this figure and the seasonal amplitude in OLR is due to the seasonal cycle in amplitude of clear sky longwave flux, which is nearly constant. Hence these results are quite similar. The seasonal amplitude in shortwave cloud forcing is shown in Figures 14a and 14b. In the tropics the amplitude and phase the of the modeled SWCF agree with the ERBE data. In the northern hemisphere summer the modeled SWCF is 25 W m^{-2} smaller than the ERBE SWCF.

Regional Comparisons

Regional comparisons are based on correlating monthly mean grid points of longwave and shortwave radiation quantities against one another. Two regions are chosen to

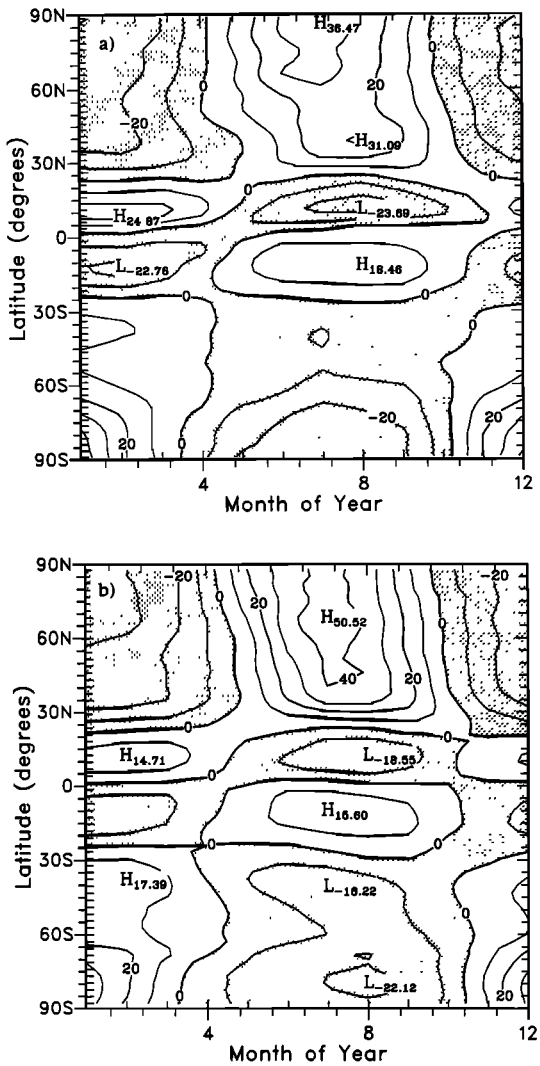

Figure 11. Seasonal amplitude in zonally averaged outgoing longwave radiation (watts per square meter) for (a) ERBE and (b) CCM2. Month 1 is January. Contour interval is 10 W m^{-2}.

exhibit the regional radiation budget. The first region is located over the tropical Pacific (10°S to 10°N, 140°E to 90°W). The second region is located over the North Atlantic storm track (30°N to 60°N, 30°W to 60°W). Similar regions were employed in the regional analysis of CCM1 by *Kiehl and Ramanathan* [1990].

The outgoing longwave flux versus albedo for July for the tropical region from ERBE and CCM2 is shown in Figures 15a and 15b. Regions of high cloud cover are represented by low OLR and high albedo. The behavior of CCM2 is reasonable; however, there appears to be more variation in the model's radiative properties than observed. In particular, the model contains a greater number of bright ($\alpha_p > 0.4$) and "cold" (OLR < 210 W m^{-2}) clouds compared to the ERBE data for this region.

Figures 16a and 16b show the longwave cloud forcing versus the shortwave cloud forcing for the same region as in Figure 15. The agreement between CCM2 and ERBE for this region is superior to the results from CCM1. Note that one source of difference may be that the ERBE data are for specific years (1986, 1988), while the CCM2 data are based on simulations employing climatological sea surface temperatures (SSTs). Indeed, there is evidence that these correlations improve when the CCM2 employs observed SSTs for the ERBE-observing period (J. J. Hack and J. T. Kiehl, manuscript in preparation, 1994).

Figures 17a and 17b present the OLR-albedo comparison for the North Atlantic storm track region. It is apparent that the model clouds are too dark compared to ERBE. ERBE albedos for this region can be as large as 0.45, while the model albedos are in general no larger than 0.35. In terms of cloud radiative forcing (Figures 18a and 18b) the SWCF in CCM2 is generally no larger than −100 W m^{-2}, whereas ERBE indicates a maximum SWCF of −150 W m^{-2}. Since most of this SWCF is deposited at the surface, the implication is that the solar flux into the ocean surface is overestimated by roughly 50 W m^{-2} for the North Atlantic region. The agreement is much better in January (not shown) where both model and ERBE SWCF reaches a maximum of −50 to −60 W m^{-2}. The implication of these regional results and

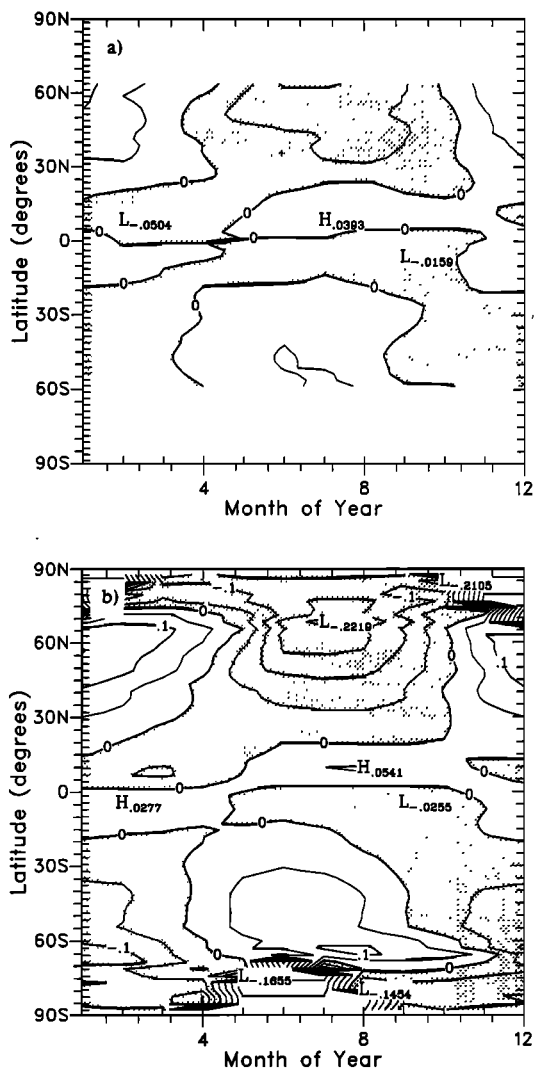

Figure 12. Seasonal amplitude in zonally averaged planetary albedo for (a) ERBE and (b) CCM2. Month 1 is January. Contour interval is 0.05.

the zonally averaged results is that in summer the cloud optical depths are too low.

5. Conclusions

This study documents the simulated Earth radiation budget of the latest version of the NCAR community climate model (CCM2). Improvements over CCM1 are most apparent in the latitudinal distribution of the longwave and shortwave cloud forcing. The correlations between longwave and shortwave radiative properties in tropics are much better in CCM2 than those reported by *Kiehl and Ramanathan* [1990] for CCM1. The phase of the seasonal cycle of the simulated Earth radiation budget is in good agreement with the observations from ERBE. However, the amplitude of the OLR cycle in the tropics is underpredicted by the model. The seasonal amplitude of SWCF in the summer hemisphere is also underpredicted. In general, the most serious bias in the simulated radiation budget is the smaller cloud forcing effects (both longwave and shortwave) in northern hemisphere summer compared to the ERBE results.

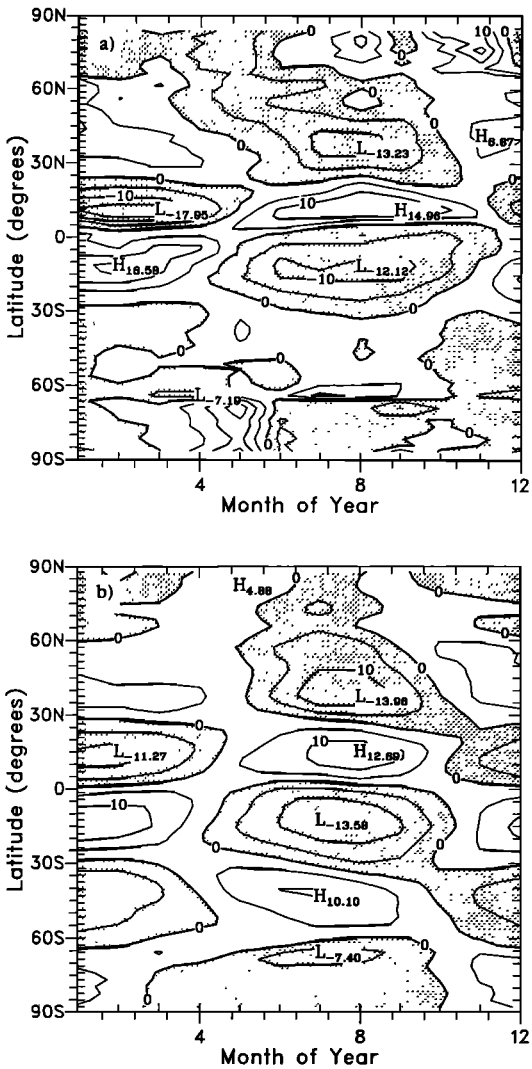

Figure 13. Seasonal amplitude in zonally averaged longwave cloud forcing (watts per square meter) for (a) ERBE and (b) CCM2. Month 1 is January. Contour interval is 5 W m^{-2}.

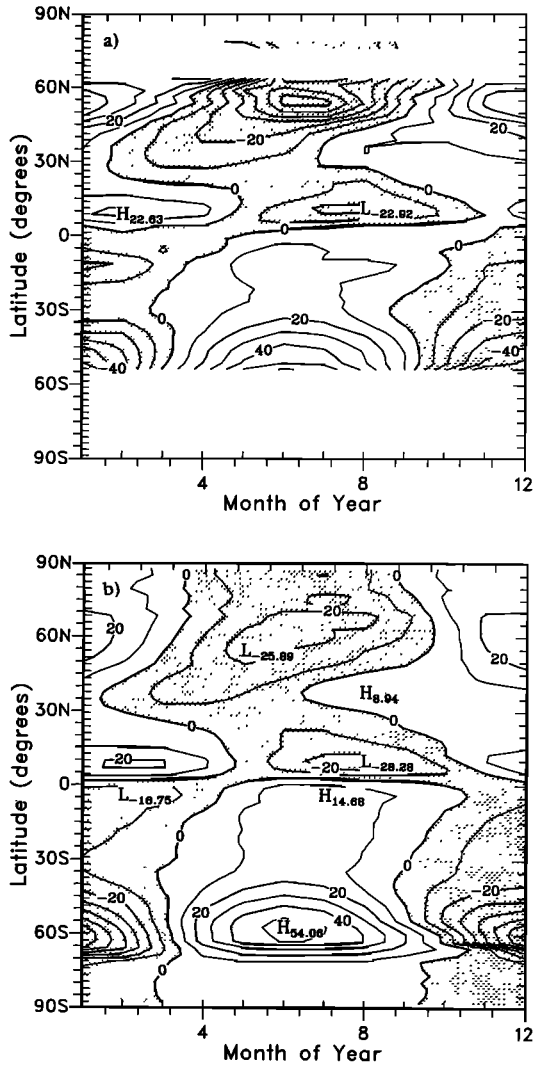

Figure 14. Seasonal amplitude in zonally averaged shortwave cloud forcing (watts per square meter) for (a) ERBE and (b) CCM2. Month 1 is January. Contour interval is 10 W m^{-2}.

This bias has now been addressed with changes to cloud optical properties. These changes are documented by J. J. Hack and J. T. Kiehl (manuscript in preparation, 1994) and *Kiehl* [1994a]. Essentially, *Kiehl* [1994a] argues that observed drop size distributions indicate that the cloud drop effective radius over northern hemisphere continental regions is 5 μm, not 10 μm as currently specified in CCM2. Use of a different effective drop size over continents and ocean eliminates roughly half of the bias in the shortwave cloud forcing. This, in turn, cools the land surface and reduces the bias in OLR. Hack and Kiehl have included a local diagnostic formulation for the liquid water scale height, h_ℓ, in (12), which results in increased liquid water paths in the summer hemisphere. This change addresses the remaining bias in the shortwave cloud forcing and significantly improves the simulated OLR.

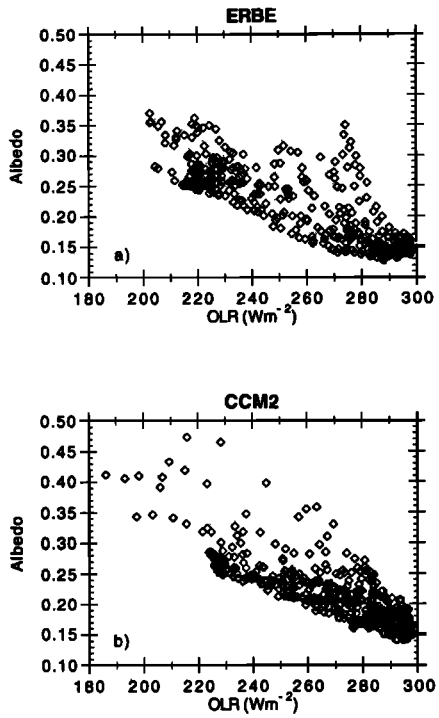

Figure 15. Planetary albedo versus outgoing longwave radiation (watts per square meter) for the tropical region (140°E to 90°W, 10°S to 10°N) for (a) ERBE and (b) CCM2.

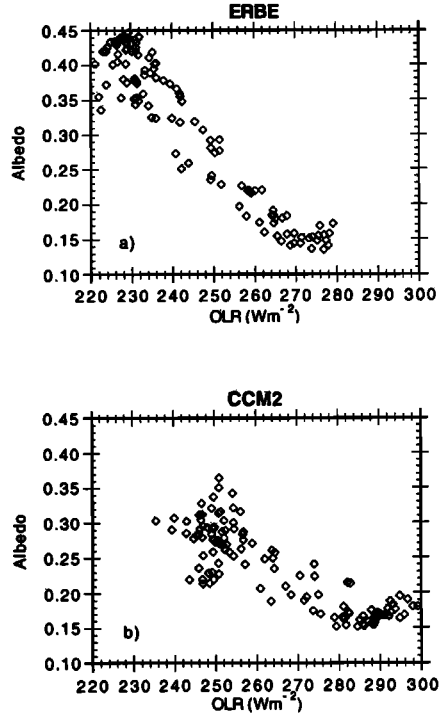

Figure 17. Planetary albedo versus outgoing longwave radiation (watts per square meter) for the North Atlantic region (30°W to 60°W, 30°N to 60°N) for (a) ERBE and (b) CCM2.

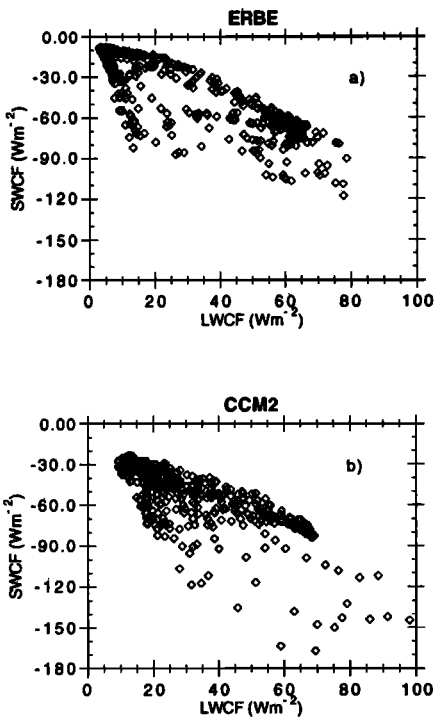

Figure 16. Shortwave cloud forcing versus longwave cloud forcing (watts per square meter) for the tropical region (140°E to 90°W, 10°S to 10°N) for (a) ERBE and (b) CCM2.

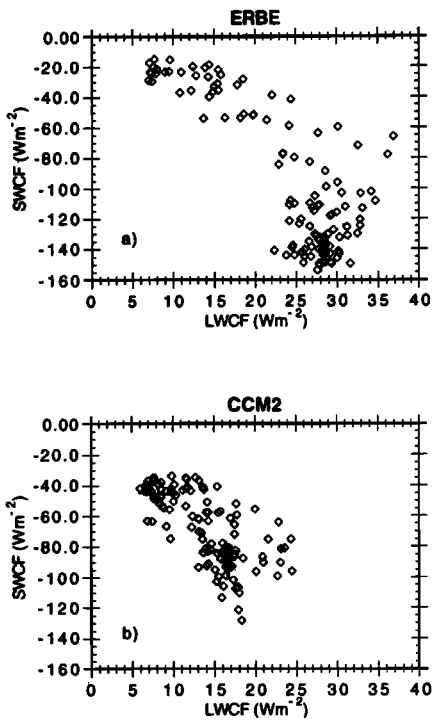

Figure 18. Shortwave cloud forcing versus longwave cloud forcing (watts per square meter) for the North Atlantic region (30°W to 60°W, 30°N to 60°N) for (a) ERBE and (b) CCM2.

Acknowledgment. The National Center for Atmospheric Research is sponsored by the National Science Foundation.

References

Barkstrom, B. R., The Earth Radiation Budget Experiment (ERBE), *Bull. Am. Meteorol. Soc.*, *65*, 1170–1185, 1984.

Barkstrom, B. R., and G. L. Smith, The Earth Radiation Budget Experiment: Science and implementation, *Rev. Geophys.*, *24*, 379–390, 1986.

Briegleb, B. P., Delta-Eddington approximation for solar radiation in the NCAR community climate model, *J. Geophys. Res.*, *97*, 7603–7612, 1992.

Cess, R. D., et al., Interpretation of cloud-climate feedback as produced by 14 atmospheric general circulation models, *Science*, *245*, 513–516, 1989.

Chylek, P., and V. Ramaswamy, Simple approximation for infrared emissivity of water clouds, *J. Atmos. Sci.*, *39*, 171–177, 1982.

Ebert, E. E., and J. A. Curry, A parameterization of ice cloud optical properties for climate models, *J. Geophys. Res.*, *97*, 3831–3836, 1992.

ERBE Science Team, First data from the Earth Radiation Budget Experiment (ERBE), *Bull. Am. Meteorol. Soc.*, *67*, 818–824, 1986.

Hack, J. J., Parameterization of moist convection in the National Center for Atmospheric Research community climate model (CCM2), *J. Geophys. Res.*, *99*, 5551–5568, 1994.

Hack, J. J., B. A. Boville, B. P. Briegleb, J. T. Kiehl, P. J. Rasch, and D. L. Williamson, Description of the NCAR community climate model (CCM2), *NCAR Tech. Note NCAR/TN-382+STR*, Natl. Center for Atmos. Res., Boulder, Colo., 1993.

Hack, J. J., B. A. Boville, J. T. Kiehl, P. J. Rasch, and D. L. Williamson, Climate statistics from the National Center for Atmospheric Research community climate model CCM2, *J. Geophys. Res.*, this issue.

Hurrell, J. W., and G. G. Campbell, Monthly mean global satellite data sets available in CCM history tape format, *NCAR Tech. Note, NCAR/TN-371+STR*, Natl. Center for Atmos. Res., Boulder, Colo., 1992.

Kiehl, J. T., Sensitivity of a general circulation model climate simulation to differences in continental versus maritime cloud drop size, *J. Geophys. Res.*, in press, 1994a.

Kiehl, J. T., On the observed near cancellation between longwave and shortwave cloud forcing in tropical regions, *J. Clim.*, *7*, 559–565, 1994b.

Kiehl, J. T., and B. P. Briegleb, A new parameterization of the absorptance due to the 15-μm band system of carbon dioxide, *J. Geophys. Res.*, *96*, 9013–9019, 1991.

Kiehl, J. T., and B. P. Briegleb, Comparison of the observed and calculated clear sky greenhouse effect: Implications for climate studies, *J. Geophys. Res.*, *97*, 10,037–10,049, 1992.

Kiehl, J. T. and V. Ramanathan, Comparison of cloud forcing derived from the Earth Radiation Budget Experiment with that simulated by the NCAR community climate model, *J. Geophys. Res.*, *95*, 11,679–11,698, 1990.

Kiehl, J. T., R. J. Wolski, B. P. Briegleb, and V. Ramanathan, Documentation of radiation and cloud routines in the NCAR community climate model (CCM1), *NCAR Tech. Note NCAR/TN-288+IA*, Natl. Center for Atmos. Res., Boulder, Colo., 1987.

Ramanathan, V., The role of Earth radiation budget studies in climate and general circulation research, *J. Geophys. Res.*, *92*, 4075–4095, 1987.

Ramanathan, V., E. J. Pitcher, R. C. Malone, and M. L. Blackmon, The response of a spectral general circulation model to refinements in radiative processes, *J. Atmos. Sci.*, *40*, 605–630, 1983.

Ramanathan, V., R. D. Cess, E. F. Harrison, P. Minnis, B. R. Barkstrom, E. Ahmad, and D. Hartmann, Cloud-radiative forcing and climate: Insights from the Earth Radiation Budget Experiment, *Science*, *243*, 57–63, 1989.

Ramaswamy, V., and S. M. Friedenreich, Solar radiative line-by-line determination of water vapor absorption and water cloud extinction in inhomogeneous atmospheres, *J. Geophys. Res.*, *96*, 9133–9157, 1991.

Shea, D. J., K. E. Trenberth, and R. W. Reynolds, A global monthly sea surface temperature climatology, *NCAR Tech. Note NCAR/TN-345+STR*, Natl. Center for Atmos. Res., Boulder, Colo., 1990.

Slingo, A., A GCM parameterization for the shortwave radiative properties of water clouds, *J. Atmos. Sci.*, *46*, 1419–1427, 1989.

Slingo, J. M., The development and verification of a cloud prediction scheme for the ECMWF model, *Q. J. R. Meteorol. Soc.*, *113*, 899–926, 1987.

Smith, L. D., and T. H. Vonder Haar, Clouds-radiation interactions in a general circulation model: Impact upon the planetary radiation balance, *J. Geophys. Res.*, *96*, 893–914, 1991.

B. P. Briegleb, J. J. Hack, and J. T. Kiehl, National Center for Atmospheric Research, P.O. Box 3000, Boulder, CO 80307.

(Received June 29, 1993; revised March 24, 1994; accepted April 5, 1994.)